The Influence of Convectively Coupled Kelvin Waves on African Easterly Waves in a Wave-Following Framework

QUINTON A. LAWTON, SHARANYA J. MAJUMDAR, KRISTA DOTTERER, CHRISTOPHER THORNCROFT, AND CARL J. SCHRECK III^c

^a Rosenstiel School of Marine and Atmospheric Science, University of Miami, Miami, Florida
 ^b University at Albany, State University of New York, Albany, New York
 ^c Cooperative Institute for Satellite Earth System Studies, North Carolina State University, Asheville, North Carolina

(Manuscript received 2 December 2021, in final form 19 March 2022)

ABSTRACT: While considerable attention has been given to how convectively coupled Kelvin waves (CCKWs) influence the genesis of tropical cyclones (TCs) in the Atlantic Ocean, less attention has been given to their direct influence on African easterly waves (AEWs). This study builds a climatology of AEW and CCKW passages from 1981 to 2019 using an AEW-following framework. Vertical and horizontal composites of these passages are developed and divided into categories based on AEW position and CCKW strength. Many of the relationships that have previously been found for TC genesis also hold true for non-developing AEWs. This includes an increase in convective coverage surrounding the AEW center in phase with the convectively enhanced ("active") CCKW crest, as well as a buildup of relative vorticity from the lower to upper troposphere following this active crest. Additionally, a new finding is that CCKWs induce specific humidity anomalies around AEWs that are qualitatively similar to those of relative vorticity. These modifications to specific humidity are more pronounced when AEWs are at lower latitudes and interacting with stronger CCKWs. While the influence of CCKWs on AEWs is mostly transient and short lived, CCKWs do modify the AEW propagation speed and westward-filtered relative vorticity, indicating that they may have some longerterm influences on the AEW life cycle. Overall, this analysis provides a more comprehensive view of the AEW-CCKW relationship than has previously been established, and supports assertions by previous studies that CCKW-associated convection, specific humidity, and vorticity may modify the favorability of AEWs to TC genesis over the Atlantic.

KEYWORDS: Africa; Atlantic Ocean; Convection; Kelvin waves; Reanalysis data; Tropical cyclones; Tropical variability; Atmospheric waves

1. Introduction

The relationship between African easterly waves (AEWs), convectively coupled Kelvin waves (CCKWs), and the formation of tropical cyclones (TCs) has been a topic of considerable interest in the past decade. Numerous studies have documented the characteristics and behavior of AEWs (Burpee 1972; Reed et al. 1977; Kiladis et al. 2006; Mekonnen et al. 2006; Hall et al. 2006; Thorncroft et al. 2008; Cheng et al. 2019), in part because these systems can serve as precursors for TCs and directly contribute to around 60% of TC genesis cases in the Atlantic (Avila et al. 2000; Chen et al. 2008; Russell et al. 2017). CCKWs, meanwhile, are equatorially trapped waves that propagate eastward (Gruber 1974; Takayabu 1994, Wheeler and Kiladis 1999; Straub and Kiladis 2002; Kiladis et al. 2009). Like AEWs, these systems modulate rainfall over Africa and the Atlantic (e.g., Mounier et al. 2007 and Mekonnen et al. 2008). While many CCKWs in the Atlantic have their origins in the Pacific (~35%), others develop over South America from in situ convection or extratropical waves (~65%) (Mayta et al. 2021; Liebmann et al. 2009).

While a plethora of research has documented the characteristics that make AEWs more or less likely to develop into

Corresponding author: Quinton A. Lawton, quinton.lawton@rsmas.miami.edu

TCs (e.g., Dunkerton et al. 2009; Hopsch et al. 2010; Berry and Thorncroft 2012; Peng et al. 2012; Leppert et al. 2013a,b; Brammer and Thorncroft 2015; Hankes et al. 2015; Russell et al. 2017; Zawislak 2020; Núñez Ocasio et al. 2020, 2021), the connection between CCKWs and TC genesis is not as well understood. Early studies initially did not find a strong global relationship between CCKWs and TCs (Frank and Roundy 2006; Bessafi and Wheeler 2006). However, subsequent workfirst done by Ventrice et al. (2012a) for the Atlantic basin and later by Schreck (2015) globally—illustrated an increase in TC genesis activity 1-2 days following the peak of CCKW-related convective enhancement (known as the "active phase"), and a reduction 0-1 days beforehand (thought to follow a convectively "suppressed" CCKW phase). Interestingly, despite the evidence that convection is essential for AEW development, this increase in TC genesis events does not occur at the peak of the convectively active phase of the CCKW. Some theories have been put forth for this lag in favorability. Ventrice et al. (2012b) studied the impact of CCKWs on environmental conditions in the Atlantic. They argued that this time period was more favorable for TC genesis due to an increase in low-level potential vorticity following the active phase, the preceding enhancement of moisture (via total column water vapor; TCWV) and convection in phase with the CCKW, as well as modifications to vertical wind shear. Using a semi-Lagrangian framework around TC genesis events, Schreck (2016) downplayed

DOI: 10.1175/MWR-D-21-0321.1

CCKW-related impacts on wind shear and moisture in favor of a progressive "buildup" of the positive vorticity anomalies following an active CCKW phase, due to the well-known westward tilt of CCKW zonal-wind anomalies with height (e.g., Straub and Kiladis 2002, 2003; Kiladis et al. 2009; Mayta et al. 2021). Schreck (2016) also noted an enhanced upper-level anticyclone following the active CCKW phase, which could enhance the outflow of preexisting disturbances. Consistent with these findings, Wu and Takahashi (2017) found that most TC genesis events connected to CCKW passages occurred north of the CCKW's anomalous low-level westerlies, a region of enhanced vorticity.

Previous research has also highlighted the influence of CCKWs on AEW initiation and growth. Ventrice and Thorncroft (2013) explored the influence of CCKWs on AEW activity via eddy kinetic energy (EKE). Following Ventrice et al. (2012b), they created composites around the passage of active phases of CCKWs through a fixed grid point near the western African coast (10°N, 15°W). They found that AEW activity increased during and after the convectively active phases of CCKWs, attributing this to convective triggering of new AEWs. There was also evidence of enhanced vorticity gradients in the AEJ core, implying that CCKWs could enhance the barotropic growth of AEWs. Building on this hypothesis, Mantripragada et al. (2021) studied the impacts of CCKWs on barotropic and baroclinic processes related to AEW growth. They fixed their analysis to the same geographic point as in Ventrice and Thorncroft (2013). Using vertically integrated perturbation kinetic energy, they found enhanced southern track AEW activity in active CCKW phases, confirming the result of Ventrice and Thorncroft (2013). Mantripragada et al. (2021) also showed that active CCKW phases enhance barotropic energy conversions (vice versa for suppressed phases). These studies suggest that CCKWs may have a long-term impact on AEW growth, although the implications for TC genesis remain unclear.

We argue that existing climatological studies on the relationship between CCKWs, AEWs, and TC genesis have substantial limitations. For one, they are often centered around TC genesis events or fixed points in the Atlantic basin. It is possible that studies centered on TC genesis events (like Schreck 2015, 2016) could be confounded by the processes specific to genesis. It is also known that the characteristics of AEWs—including convection—look and behave differently depending on longitude (e.g., our Fig. 2; Hopsch et al. 2010; Brammer and Thorncroft 2015; Janiga and Thorncroft 2016; Russell and Aiyyer 2020). Thus, results centered at a specific geographic point may not be representative of other locations. Additionally, existing studies of CCKW and AEW interactions have focused heavily on AEW growth processes but not as much on other characteristics pertinent to AEW behavior, including AEW propagation speed and structure. For example, the relationship between CCKWs and specific humidity within AEWs has not been explored in detail. While a few of these environmental variables have been considered in TC genesis or CCKW centered studies (e.g., Ventrice et al. 2012a,b; Ventrice and Thorncroft 2013; Schreck 2015, 2016), AEWs are important in their own right even if they do not develop into TCs. Investigating the AEW-CCKW relationship

TABLE 1. Selected statistics from the AEW tracker used in this study, run over the years 1981–2019 for months July–September. For developers, track length and time duration only include the AEW track prior to TC genesis. Track length is computed as the maximum minus the minimum tracked longitude. Unlike later analysis, statistics are not limited by the AEW position in longitude or latitude.

	Non-developers	Developers	
Total AEW count	1236	185	
Mean count per season	31.7	4.8	
Mean track length	43.7	50.2	
(degrees longitude)			
Median track length	38.5	49.0	
(degrees longitude)			
Mean wave duration (days)	7.1	8.2	
Median wave duration (days)	6.0	8.0	
Mean westward propagation	8.0	7.8	
speed (m s ⁻¹)			

from an *AEW-following perspective* provides an opportunity to better isolate the impacts of CCKWs on AEW behavior. It also allows for the comparison of AEW-CCKW interactions between different geographical regions.

In this paper, we expand beyond the aforementioned studies by using an AEW-following framework to build a climatology of AEW-CCKW interactions for the years 1981–2019. To address limitations in the earlier studies, we use an objective AEW tracker to follow AEWs as they pass CCKWs and limit our analysis to AEWs that do not become TCs. This AEW-centered framework allows us to easily compare the impacts of CCKWs on AEWs for different regions and for varying wave strengths. Our goals are as follows: 1) to improve our understanding of how CCKWs modify AEWs and consolidate previous hypotheses in an AEW-following framework, 2) to better attribute these results to CCKW and AEW wave processes, and 3) to illuminate how differences in location and wave characteristics impact the AEW-CCKW relationship.

2. Data and methods

a. Data

The environmental fields used for composites and AEW tracking are obtained from global fifth-generation ECMWF reanalysis (ERA5) data (Hersbach et al. 2020). The large time period (1981–2019) necessitates that the ERA5 data be downsampled to a $1^{\circ} \times 1^{\circ}$ grid, 19 pressure levels (1000–100 hPa), and a 6-hourly temporal resolution. Satellite brightness temperature data for CCKW identification are obtained from the NOAA GridSat-B1 dataset (Knapp et al. 2011, data henceforth referred to as T_b). For computational efficiency, the satellite data are downsampled to a $0.25^{\circ} \times 0.25^{\circ}$ grid.

A 41-yr climatology (1979–2019) of environmental data is constructed. The first four harmonics of the mean annual cycle for each 6-h period are computed, following Brammer and Thorncroft (2015). With the exception of the heating and vorticity fields, most environmental data are computed as anomalies about this climatology.

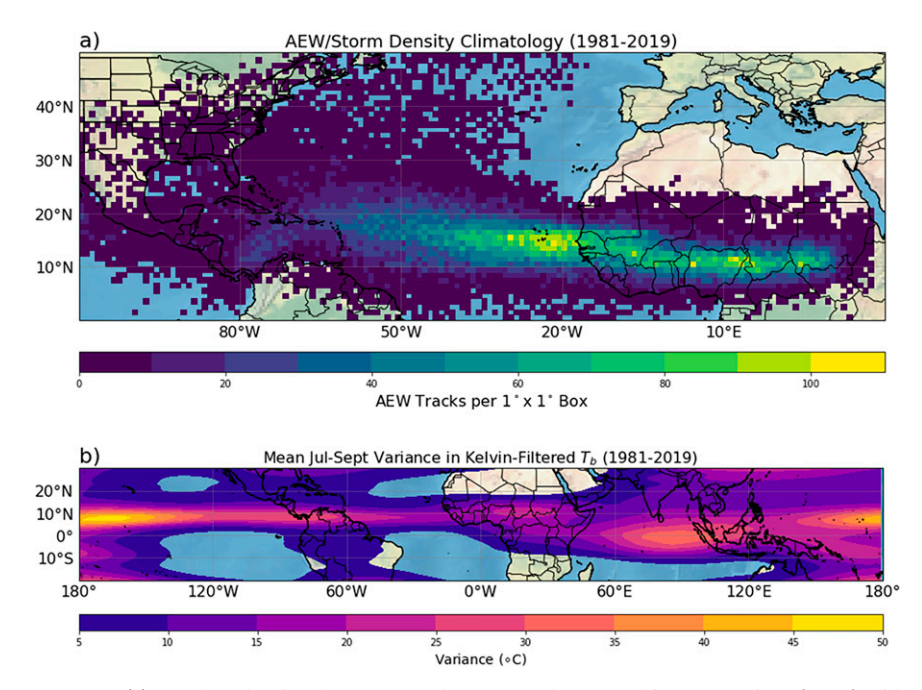


FIG. 1. (a) Number density plot of tracked AEWs and any resulting TCs, using $1^{\circ} \times 1^{\circ}$ grid boxes across a 1981–2019 climatology for the months July–September. (b) Variance of Kelvin-filtered T_b for the months July–September averaged over the years 1981–2019.

b. AEW tracking

The AEW tracker developed for use in this study is similar to that of Brammer and Thorncroft (2015) and Elless and Torn (2018). As was shown by Berry et al. (2007) and subsequent work, curvature vorticity at 700 hPa is useful for AEW tracking as it excludes shear-induced vorticity (such as that arising from the African easterly jet). We utilize a "modified" curvature vorticity (CV) where we compute CV using the *nondivergent* component of the 700-hPa wind, and then average it within a radius of 600 km of each grid point.

Following Elless and Torn (2018), AEWs are identified over land using meridional averages of CV. This method is effective at identifying AEW centers over Africa. Over the ocean, however, a technique more like that of Brammer and Thorncroft (2015) must be used. There, an AEW's velocity is used to estimate its position at the next time step. In both cases, a weighed centroid technique is run on the CV field to determine the final position of the AEW center. In our analysis, we only consider waves that have a known origin over the African continent and are tracked for at least 2 days. We also exclude all AEWs connected to a TC genesis event. These "developing" AEWs are identified by checking if an AEW center is located within 500 km of a TC genesis point in the HURDAT dataset (Landsea and Franklin 2013). The AEW tracks used in our analysis and detailed code documentation are provided in an online data repository (see data availability statement).

Statistics from the AEW tracking database are provided in Table 1. Many of the tracked AEWs are long lived, with an average duration of a week and an average track spanning over 43° longitude, though this is inflated by long-tracking outliers. The average of 36.5 tracked AEWs per season is equal to or

higher than several other objective AEW trackers that captured an average of 26–36 AEWs per season (Bain et al. 2014; Hopsch et al. 2010; Berry et al. 2007). A qualitative inspection of tracks within each year (not shown) indicates that dropped or missed AEW tracks are exceedingly rare, and that the vast majority of TC genesis events from AEWs in the Main Development Region are captured.¹

As illustrated by the AEW density plot in Fig. 1a, most identified waves over Africa are located between 10° and 15°N, suggesting they originate within the southern formation track. The track density is similar to that produced by the Brammer and Thorncroft (2015) tracker (cf. their Fig. 2), with most AEW activity concentrated over West Africa or just off the African coast. However, some AEWs can make it into the eastern Pacific or recurve into the North Atlantic as TCs. These regions are not included in our analysis.

Characteristics of tracked AEWs compare well with existing AEW studies. The average westward propagation speed of non-developing AEWs from longitudes 20°E–40°W (Table 1) is nearly identical to the 8 m s⁻¹ propagation speed identified by Reed et al. (1977). Composites of AEW structure (Fig. 2)

¹ This can be quantified via a "success rate" for capturing genesis events, defined as the number of detected TC genesis events captured in the tracker divided by the total number of TC genesis events in the HURDAT database. For the years 1979−2019, this tracker identified 75% of all TC geneses east of 60°W, increasing to 83% when waves with oceanic origins are included. Considering that some of the "missed" TC geneses may have complicated origins (multiple AEWs, ITCZ generation, etc.), this suggests the tracker captures the vast majority of traditional developing AEW events.

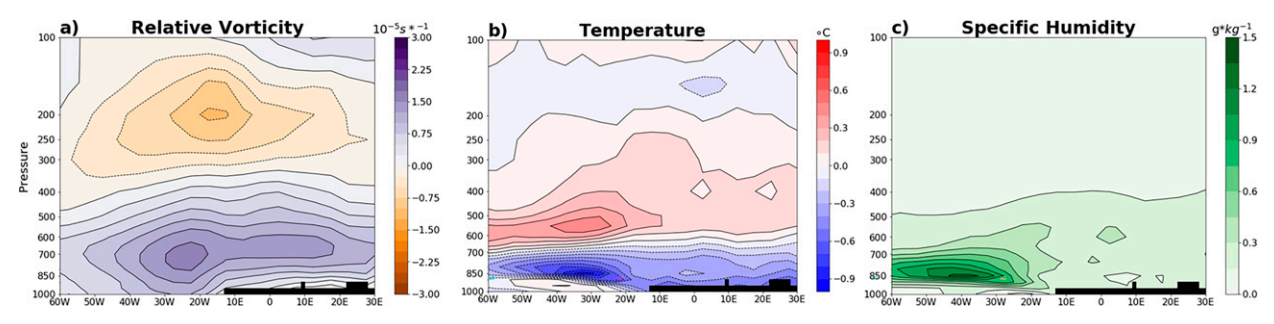


FIG. 2. Climatology of (a) relative vorticity, (b) temperature anomalies, and (c) specific humidity anomalies averaged within 600 km of the tracked AEW centers. Vertical slices of these averages are composited every 5° longitude. These composites include only non-developing AEWs that can be tracked back to the African continent. Grid boxes where pressure levels are typically located below the surface are blacked out.

in longitude are also consistent with previous studies and wave trackers. Relative vorticity is concentrated between 700 and 600 hPa and is strongest for AEWs located just off the coast of Africa (20°-30°W; Fig. 2a). As AEWs move away from the coast, their vorticity structures deepen at lower levels, as shown in previous studies (Janiga and Thorncroft 2013; Brammer and Thorncroft 2015; Russell and Aiyyer 2020). Composite temperature anomalies are consistent with this 700-600-hPa vorticity maximum, with cold anomalies generally located below 700-650 hPa and warm anomalies above (Fig. 2b). These temperature anomalies increase in magnitude where vorticity increases, as expected via the thermal wind relation. Furthermore, specific humidity is concentrated from 850 to 700 hPa and is enhanced for AEWs over the Atlantic as compared to land (Fig. 2c).

c. Spatiotemporal filtering and CCKW identification

To identify CCKWs, we first filter in space and time in the Kelvin band following the method of Wheeler and Kiladis (1999). The Kelvin wave filter bounds a temporal period of 2.5–20 days, a zonal wavenumber of 1–14, and an equivalent depth of 8–90 m. We apply this filter to the T_b dataset each year from June to October, and then cut the data length down to July–September.

The mean variance of Kelvin-filtered T_b from July to September, shown in Fig. 1b, has a similar distribution to that found in previous studies for convection or rainfall-related fields [cf. Fig. 1 from Mayta et al. (2021) and Fig. 1 from Schreck (2015)]. Local maxima in variance are located in the Indian and Pacific Ocean basins. In the Atlantic, CCKW activity is displaced slightly north of the equator with reduced variance compared with many other ocean basins. Due to the observed northward displacement, we use the 0° - 10° N average of Kelvin-filtered fields for CCKW identification and a 1.0 standard deviation threshold, consistent with Schreck (2015).

Later in our analysis, we use a different filter on the ERA5 fields to separate CCKW contributions (eastward signals) from AEW responses (westward signals). This filter foregoes temporal filtering entirely and encompasses a large range of zonal wavenumbers in an attempt to capture the full range of signals

 $(-99\,999\,\text{to}\,-1\text{ for westward propagation and }1\text{ to }99\,999\text{ for eastward propagation}).$

d. Building AEW-CCKW lagged composites

The tracked AEWs and Kelvin-filtered fields are leveraged to build a database of AEW-CCKW passages from 1981 to 2019 for the months July-September. Figure 3 illustrates this process using a single AEW-CCKW passage in 1995 as an example.

- Position, strength, and environmental data for a single AEW track are loaded from our AEW database. The black line in Fig. 3a depicts the track of wave 19 in 1995.
- 2) "Crests" of active and suppressed phases of CCKWs are identified relative to the AEW using the Kelvin-filtered T_b fields. To do so, we identify the longitude of the AEW center at a given time step. The Kelvin-filtered T_b field is averaged from 0° to 10°N at this same longitude. This process is repeated for the entirety of an AEW's lifetime. We then identify CCKW crests via local minima/maxima in this field that exceed ±1 standard deviation (as computed for the period July–September from 1981 to 2019) at that longitude. An example of this process is shown in Fig. 3b, with the final locations of identified CCKW crests shown as blue/red triangles.
- 3) We save AEW characteristics and environmental data for the time period surrounding each CCKW crest: this slice extends from 3 days beforehand and 3 days afterward. "Day 0" refers to the point in time when the center of the tracked AEW aligns in longitude with a CCKW crest. Figure 3c shows an example of this for TCWV averaged within 600 km of a AEW as it passes an active CCKW crest (the blue triangle).
- 4) We subtract the AEW-relative climatology (in longitude) from the data in step 3 to adjust for the changes in AEW characteristics that typically occur for different longitudes (e.g., Fig. 2). This AEW-relative climatology is computed over the entire database (1981–2019). It should be noted that this adjustment step is not done for spatial composites in section 3c. However, when this step was tested for select spatial composites (specific humidity and vorticity), we found it had no our effect on our final conclusions.

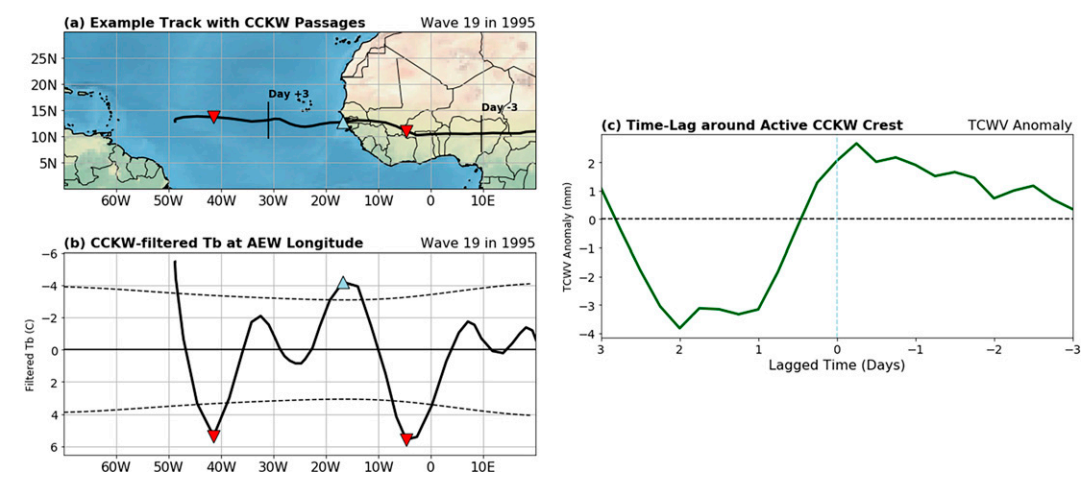


FIG. 3. Example of the AEW–CCKW compositing methodology utilized in this study. (a) The black line shows the analyzed track of wave 19 in 1995, with red triangles (pointed down) indicating the location of the AEW when it passed a suppressed crest of a CCKW, and the blue triangle (pointed up) when it passes an active crest. (b) The Kelvin-filtered T_b averaged between 0° and 10° N at the same longitude as the tracked AEW, with corresponding triangles (red for suppressed phase; blue for active phase) showing objectively analyzed CCKW crests, corresponding to the triangles in (a). (c) The TCWV averaged within 600 km of the AEW over a 6-day time period surrounding the passage of an active CCKW crest [blue triangle in (a) and (b)]. The x axis here is flipped, with the location of the AEW at the beginning (day -3) and end (day +3) of this time series plotted as vertical black lines in (a).

5) These steps are repeated for every tracked AEW in the database. Composites are generated by averaging across either all the samples or a subset of samples.

We only consider AEW-CCKW passages that occur in a box bounded by 0°-20°N, 60°W-30°E (see Fig. 4a). Because

active and suppressed composites are computed separately and compared, it is important to check for any biases in the sampled passages in each group. This is highlighted by the passage location markers and histograms in Fig. 4. For the most part, there do not appear to be major differences in the positional distribution of active- and suppressed-phase CCKW interactions.

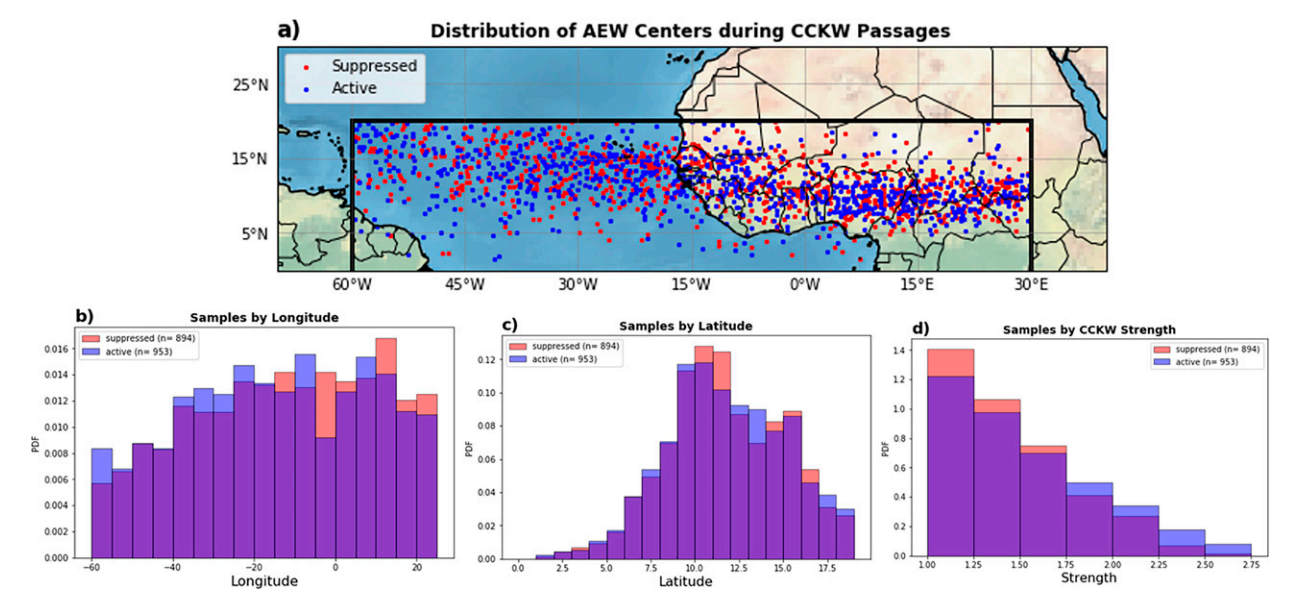


FIG. 4. Comparison of the distribution of samples included for the active and suppressed composites. (a) Location of the tracked AEW centers for all AEW–CCKW passages in this analysis, with red dots indicating samples for suppressed CCKW crests and blue dots for active CCKW crests. (b) Normalized PDF distribution comparing active and suppressed samples by longitude of the AEW center, with red indicating samples for suppressed CCKWs, blue for active CCKWs (purple is the overlap). (c) As in (b), but binned by latitude of the AEW center. (d) As in (b), but binned by CCKW strength in standard deviation.

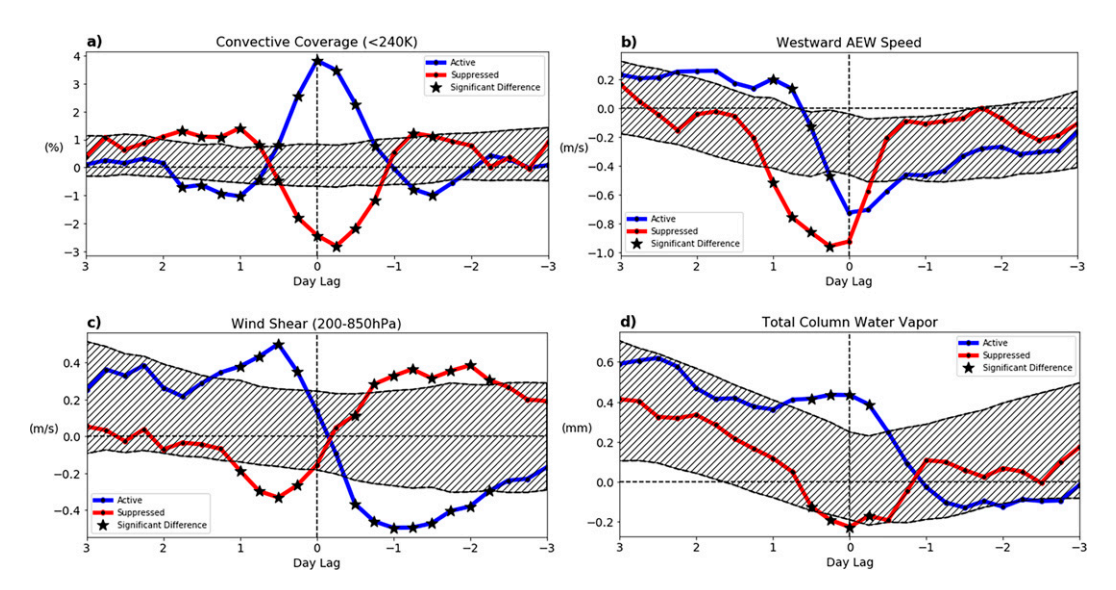


FIG. 5. Lagged comparisons of composited data surrounding AEWs as they pass through active or suppressed CCKWs for (a) convective coverage as indicated by the percentage of area within 600 km of the AEW center with T_b values below 240 K, (b) westward propagation speed of AEWs, (c) 200–850-hPa wind shear magnitude averaged within 600-km of the AEW center, and (d) TCWV averaged within 600 km of the AEW center. Data are rotated relative to the longitudinal passage of CCKW crests, such that day 0 is when the AEW is aligned in longitude with the crest of the CCKW. Red lines indicate composites surrounding suppressed CCKW crests, and blue lines indicate composites surrounding active CCKW crests. The gray hatched region is the 95% confidence interval generated by composites with randomized day 0 points (null hypothesis 1); since they slightly differ based on composite type, the widest (most restrictive) interval is plotted. Stars indicate where active and suppressed composites are significantly different from one another at a 95% level (null hypothesis 2).

One exception is a slight shift in concentration of suppressed phase passages eastward, over land (Fig. 4b). Interestingly, active-phase passages appear slightly stronger on average compared to their suppressed-phase counterparts (Fig. 4d), which could be a result of using a fixed one standard deviation interval. AEWs move slightly poleward as they transit the Atlantic (Fig. 1a) and thus AEWs tend to pass CCKWs at higher latitudes over the western portion of the study region (Fig. 4a).

e. Statistical significance for lagged composites

In our analysis, we identify two null hypotheses for testing the significance of lagged AEW-CCKW composites. Each is distinct with slightly different interpretations.

The first concerns the selection of CCKW crests at the day 0 lag time, and is referred to as "null hypothesis 1." Null hypothesis 1 posits that centering composites around CCKW crests (i.e., day 0) produces results indistinguishable from those produced when choosing random times along an AEW track as the day 0 center instead. To test this, we build 1000 random composites using the same method as the original, but this time choosing random points along each AEW's track to serve as the day 0 time instead of the CCKW crest. For each random composite, the same AEWs and number of samples are chosen as in the original. This bootstrapping-like methodology is necessary to account for some biases, including differences in the sample size at different lag times, which result from the compositing itself. To reject null hypothesis 1 at a 95% threshold, the active or suppressed composite values must

be above or below that of 975 of the 1000 randomly generated composites.

The second null hypothesis is that the active and suppressed composites are the same for a given composite time, and is henceforth referred to as "null hypothesis 2." To evaluate this, we use a bootstrapping method to create 1000 (or 10000 for single-level parameters) subsets from the active and suppressed composites. Each subset composite randomly samples waves from the original active or suppressed composite with replacement. We reject the null hypothesis at a 95% level if 975 of the bootstrapped active composites are greater or less than 975 of the bootstrapped suppressed composites. This method is slightly modified for the regional and strength composite groupings shown in section 3e. For these groupings, we are interested in the net magnitude of the active-suppressed difference itself. Thus, bootstrapping is run with the random subsets taken from the net difference between active and suppressed composites. This is referred to as "modified null hypothesis 2."

One caveat is that the propagation speeds of individual AEWs and CCKWs vary, causing the AEW positions relative to passing CCKWs to move out of phase with one another as they get further out from day 0. This could make it more difficult for composites to clear significance at larger lag times (±2 days) but should not influence the core conclusions presented here. Additionally, AEW samples may occasionally show up at more than one time lag if passing through multiple, same-signed CCKW crests. Sensitivity

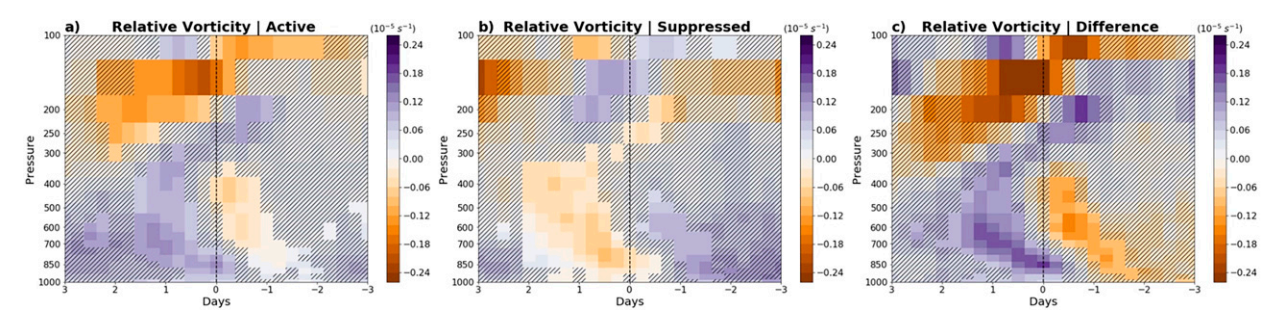


FIG. 6. Vertical cross sections of the relative vorticity averaged within 600 km of the AEW center, lagged relative to CCKW crests. (a) The composite surrounding active CCKW crests and (b) the composite surrounding suppressed CCKW crests. Regions that are not significantly different from random composites at a 95% threshold are hatched out (null hypothesis 1). (c) The difference in the active and suppressed composites [(a) minus (b)]: areas where these two composites are not significantly different from one another at a 95% threshold are hatched out (null hypothesis 2). The *x* axis is flipped such that positive lags (after the CCKW crests) are on the left and negative lags (before the CCKW crests) are on the right—this makes the vertical cross sections more consistent with a zonal slice.

tests were conducted where these overlapping, with no notable impacts on our final conclusions. Results discussed here passed significance tests for both null hypotheses 1 and 2, indicating the final conclusions are robust.

3. Composite characteristics of AEW-CCKW passages

First, we present and interpret time-lagged composites taken over the entire geographic region of study (30°E-60°W). This is done to give a sense of the evolution of AEW characteristics as they move through CCKWs over the whole study domain. Three types of composites are analyzed. Single-level composites (section 3a) detail the response of AEW behavior and integrated quantities to AEW-CCKW interactions, vertical composites (section 3b) demonstrate the vertical extent of any environmental response, and spatial composites (section 3c) illustrate where variables change relative to the AEW center. We primarily focus on environmental fields important to AEW dynamics and impacts: various measures of humidity, relative vorticity, large-scale flow, and convection. Composites in this section are not filtered in space or time, meaning they include the superposition of both the AEW and CCKW signals.

a. Single-level composites

Figure 5a shows composites of areal convective coverage for a 600-km circle surrounding the AEW center. The choice of convective coverage rather than intensity here is deliberate; previous studies have indicated that increased spatial coverage of convection and precipitation is important for TC genesis from AEWs (Leppert et al. 2013a,b; Brammer et al. 2018; Zawislak 2020). We follow these studies in using $T_b = 240 \text{ K}$ as a threshold for this purpose. Convective activity surrounding the AEW increases significantly near day 0 (CCKW crest) when moving through an active phase, and vice versa for the suppressed phase. Another important feature in Fig. 5a is a weaker signal in the opposing direction 1–2 days before and after day 0. This is because CCKW phases are often preceded and/or followed by the opposite phase.

Figure 5b illustrates the composite change in the westward component of AEW propagation speed as AEWs pass through CCKWs. There is a strong decrease in the AEW propagation speed during and following a suppressed CCKW crest, lasting for up to a day. Meanwhile, AEWs moving through an active crest also experience a decrease in propagation speed before and during the crest, but at slightly earlier lag times than the suppressed composite. This initial decrease in the active composite is followed by an increase in propagation speed from +0.75 days (18 h) through +2 days. One interpretation of this result is that the initial decrease in AEW speed corresponds with the passage of a suppressed crest at days -2 through -1. In both cases, the decrease in the AEW propagation speed is the most prominent signal, approaching magnitudes of -0.8 m s^{-1} , which is $\sim 10\%$ of the typical AEW propagation speed.

Previous work on AEW propagation gives credence to this being a physically relevant behavior. Russell et al. (2020) noted that changes in AEW propagation appeared to occur in "bursts" in relation to convective activity. Furthermore, Russell and Aiyyer (2020) illustrated that deep convection is essential to resisting deformation of the AEW vorticity by the background vertical wind shear and keeping the system vertically coupled, though they did not test what impact this has on total AEW speed. A cause of the observed decrease in AEW speed could be that the reduced convective activity of the suppressed phase both: 1) directly diminishes convectionrelated propagation, and 2) causes the middle and upper levels (with strong background easterlies) of the AEW to decouple from the lower levels (weak background easterlies or even westerlies). Supporting this theory is that we find a weaker relationship in AEW speed for AEW-CCKW passages between 60° and 40°W, where AEW-related convection is often weaker and contributes less to AEW propagation dynamics (Russell and Aiyyer 2020; Janiga and Thorncroft 2016). Another theory is that, if AEWs were to behave like many convectively coupled equatorial waves (e.g., Emanuel et al. 1994; Kiladis et al. 2009), an increase in convection prior to and during the active CCKW phase could further couple to the AEW and reduce its speed. However, this would not explain the

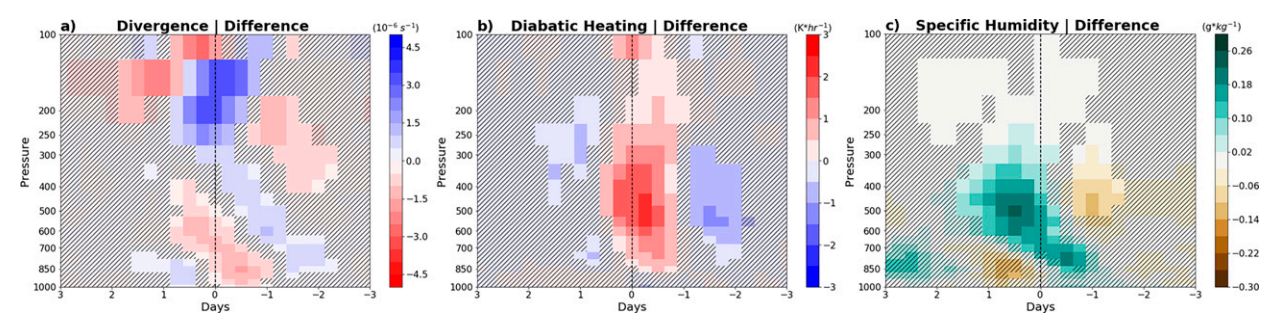


FIG. 7. As in Fig. 6c, but for (a) divergence, (b) diabatic heating, and (c) specific humidity all averaged within 600 km of the AEW center. Diabatic heating is estimated by the thermodynamic residual and is referred to as Q_1 . Significance testing is done here via null hypothesis 2.

observed reductions in speed associated with suppressed CCKW crests.

The behaviors of wind shear magnitude and TCWV illustrated in AEW-CCKW composites (Figs. 5c,d) are similar to those found by Ventrice et al. (2012b) for CCKW-centered composites. TCWV surrounding the AEW changes in phase with the CCKW crest around day 0, increasing in active composites and decreasing in suppressed composites (Fig. 5c). Wind shear surrounding the AEW increases following an active CCKW crest and decreases following a suppressed crest, for up to a day (Fig. 5d). The magnitude of these changes is relatively small. As Schreck (2016) argued for pre-TC disturbances, CCKW-induced zonal wind anomalies likely contribute less to wind shear near the AEW due to the poleward displacement of AEWs from equatorially trapped CCKWs. Additionally, the longitudinal extent of AEW-CCKW passages considered for this composite encompasses multiple background shear regimes that the CCKW will contribute to differently. This is further explored in section 4.

b. Vertical cross-section composites

Vertical cross sections of composited relative vorticity surrounding AEWs are constructed for active and suppressed CCKW passages versus climatology (Figs. 6a,b), and for the difference between the active and suppressed composites (Fig. 6c). A lagged relationship in height is apparent. At the time of the active-CCKW crest passage, vorticity first increases at lower levels (700-1000 hPa) from 0 to +1 day (Fig. 6a). Starting +0.75 days (18 h) following the active crest, this increase in vorticity begins shifting higher up in the troposphere (300-700 hPa), until significant changes finally subside near day +1.75. Prior to the CCKW passage, there is a similar structure of reduced vertical vorticity that likely corresponds to a preceding suppressed CCKW phase. The suppressed composite (Fig. 6b) is similar to the active-phase composite but reversed. Near and above the tropopause (200–100 hPa), changes in vorticity are reversed compared with those at lower levels, with an anticyclonic (negative) relative vorticity anomaly. These vorticity changes lag behind regions of convergence and divergence (Fig. 7a).

An important observation is that Fig. 6a and Fig. 6b are effectively opposite in phase of each another. This behavior was not isolated to relative vorticity; it was true for every other

vertical composite generated (not shown). This allows us to focus on the difference plots for these vertical composites.

Differences between active and suppressed composites for other parameters surrounding the AEW are shown in Fig. 7. Diabatic heating is estimated from the thermodynamic residual, a quantity referred to as Q_1 (Yanai et al. 1973; Russell and Aiyyer 2020). The Q_1 computed from reanalyses was shown by Russell and Aiyyer (2020) to be a fair estimate of diabatic heating in AEWs. As expected, Fig. 7b highlights that there is more diabatic heating in the active composites than the suppressed composites in a vertically extensive column from day -1 through day +0.5. Vertical gradients in Q_1 suggest that diabatic heating could be temporarily increasing the potential vorticity at low levels (and thus, the relative vorticity) and decreasing it near the tropopause for active CCKW passages (vice versa for the suppressed CCKW phase passage).

The change in specific humidity anomalies (Fig. 7c) surrounding AEWs is strikingly similar to what was found for vorticity in Fig. 6c. Statistically significant differences in specific humidity between the composites begin 0.75-0.5 days prior to the CCKW crest at low levels (850-700 hPa), and then transition to mid- and upper levels quickly following the CCKW-crest passage, lasting for up to +1.5 days. This lagged response and variation with height suggests that TCWV is not fully representative of CCKW-related modifications in moisture (cf. Fig. 5d and the results of Ventrice et al. 2012b). The enhancement of active-phase specific humidity at upper levels is partially countered by a decrease at lower levels, masking this signal in TCWV composites. There is a corresponding decrease in temperature (not shown) at the same time of the increased specific humidity, implying an increase in relative humidity.

Overall, these vertical composites have striking similarities to previous studies. Changes in vorticity (Fig. 6) were consistent with the processes Schreck (2016) argued are important for pre-TC disturbances.² Our results for specific humidity (Fig. 7c) and temperature (not shown) are also similar to vertical composites

² This can be compared to the vertical cross sections of zonal-wind anomalies, relative to TC-genesis, taken by Schreck (2016) in the eastern Pacific at low latitudes (their Fig. 2). Their results for zonal wind imply a similar modification to vorticity as our results do for AEWs, but in their case for TC precursor disturbances.

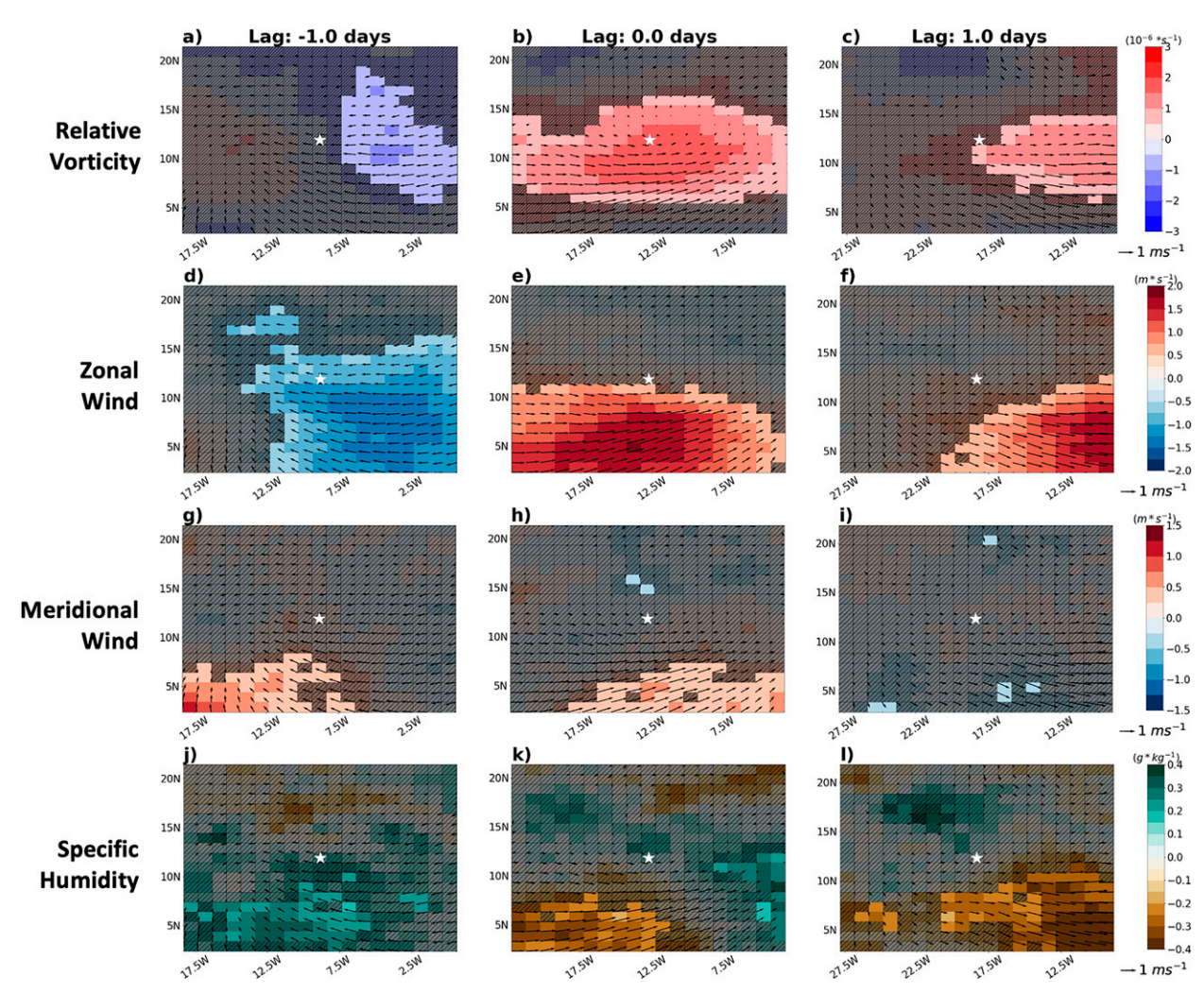


FIG. 8. Lagged differences in spatial composites of variables in a $20^{\circ} \times 20^{\circ}$ box surrounding AEW centers at 850 hPa. Differences (active minus suppressed composites) are shown, with data grayed out and hatched where the active composites are not significantly different from suppressed composites at a 95% threshold (null hypothesis 2). Each column is a different time relative to the CCKW crest passage: (from left to right) differences for 1 day before the CCKW crest, for day 0, and for 1 day following the CCKW crest. (a)–(c) Differences in smoothed relative vorticity, which is smoothed by computing a 600-km radial average surrounding each grid box. (d)–(f) Zonal wind, (g)–(i) meridional wind, and (j)–(l) specific humidity. The overlain black vectors indicate the difference in the 850-hPa wind between the active and suppressed composites. Latitude and longitude values are only shown for reference, as each sample is rotated to the average latitude and longitudes of the entire dataset.

of these quantities taken from observations and reanalysis constructions of CCKWs (Straub and Kiladis 2002, 2003; Kiladis et al. 2009; Mayta et al. 2021).

c. Spatial composites

We now discuss differences in $20^{\circ} \times 20^{\circ}$ spatial composites surrounding AEWs. The 850- and 400-hPa levels are highlighted as each is representative of low-level and mid- to upper-level changes, respectively.

Differences in the spatial composites for 850-hPa vorticity and the related zonal and meridional wind components (Figs. 8a-i) support the sequence of events depicted by the vertical composites. One day before reaching an active CCKW crest, relative vorticity is reduced in the vicinity of

the AEW center (Fig. 8a). This change appears largely driven by zonal wind anomalies at and equatorward of the AEW center (Fig. 8d). As the AEW transitions to be in phase with the active CCKW crest (day 0), the zonal wind anomalies change direction and relative vorticity is enhanced surrounding the AEW center (Figs. 8b,e). One day following the CCKW crest, these vorticity and zonal wind anomalies are displaced eastward away from the AEW center (Figs. 8c,f). Observed changes in zonal wind are consistent with the zonal wind anomalies that have previously been observed for CCKWs across the globe (e.g., Kiladis et al. 2009; Mayta et al. 2021), and compares quite well to what Schreck (2016) illustrated for incipient TC-disturbances passing CCKWs (cf. their Figs. 2 and 3). Meanwhile, meridional

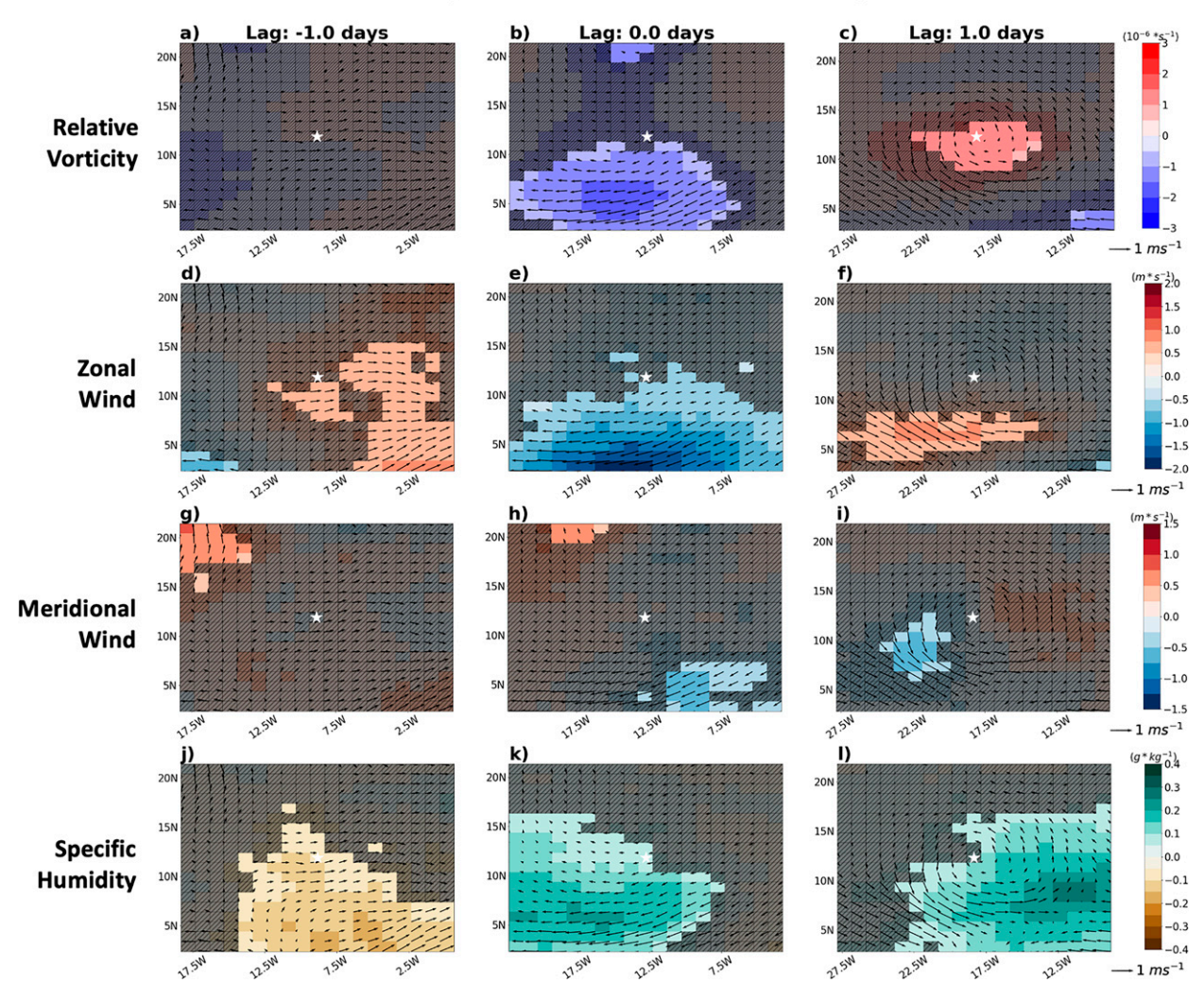


FIG. 9. As in Fig. 8, but at 400 hPa.

wind anomalies (Figs. 8g-i) are displaced equatorward from the AEW center at this level.

Differences in the spatial composites at 400 hPa are also consistent with the tilted response seen in the vertical composites. Initially, relative vorticity is not significantly different one day prior to the CCKW crest (Fig. 9a). By the time the AEW is collocated with the active CCKW crest (Fig. 9b), a large swath of reduced relative vorticity is located south of the AEW center, followed by an increase in relative vorticity on day +1 (Fig. 9c). The zonal wind and vorticity composites shown here for 400 hPa are similar to those depicted by Schreck (2016) at 500 hPa for TC genesis cases.

CCKW-induced 400-hPa zonal wind anomalies south of the AEW center (Figs. 9d–f) appear to play a role in modulating relative vorticity. However, on day +1, there is a region of significantly enhanced northerlies west and southwest of the AEW center (Fig. 9i), much closer to the AEW than any of the meridional anomalies seen at the 850-hPa level. The wind vector differences on day +1 are suggestive of a cyclonic

circulation anomaly collocated with the AEW center. This is distinct from the primarily zonal wind contribution to relative vorticity seen at 850 hPa at the same time. This could indicate a dynamical response of the AEW to the increased convective coverage on day 0 (Fig. 5a) and higher specific humidity (Fig. 91).

The time sequence of 400- and 850-hPa spatial composites for specific humidity (Figs. 8j–l, 9j–l) is qualitatively similar to vertical composites (Fig. 7c). Unlike the 850-hPa composites, however, specific humidity differences at 400-hPa encompass the AEW center and even regions north of it. A comparison between the 850- and 400-hPa-level composite differences at ±0.75 days (±18 h) emphasizes this point (Fig. 10). Several factors could be contributing to the differences in spatial extent for the specific humidity response. For one, consider the AEW-relative recirculation. At 850 hPa, relative vorticity is most enhanced when the AEW is aligned with an active CCKW crest (Fig. 8b) and appears to be driven primarily by zonal wind shear anomalies. While this is likely helping to strengthen the westerlies contributing to the wave "pouch"

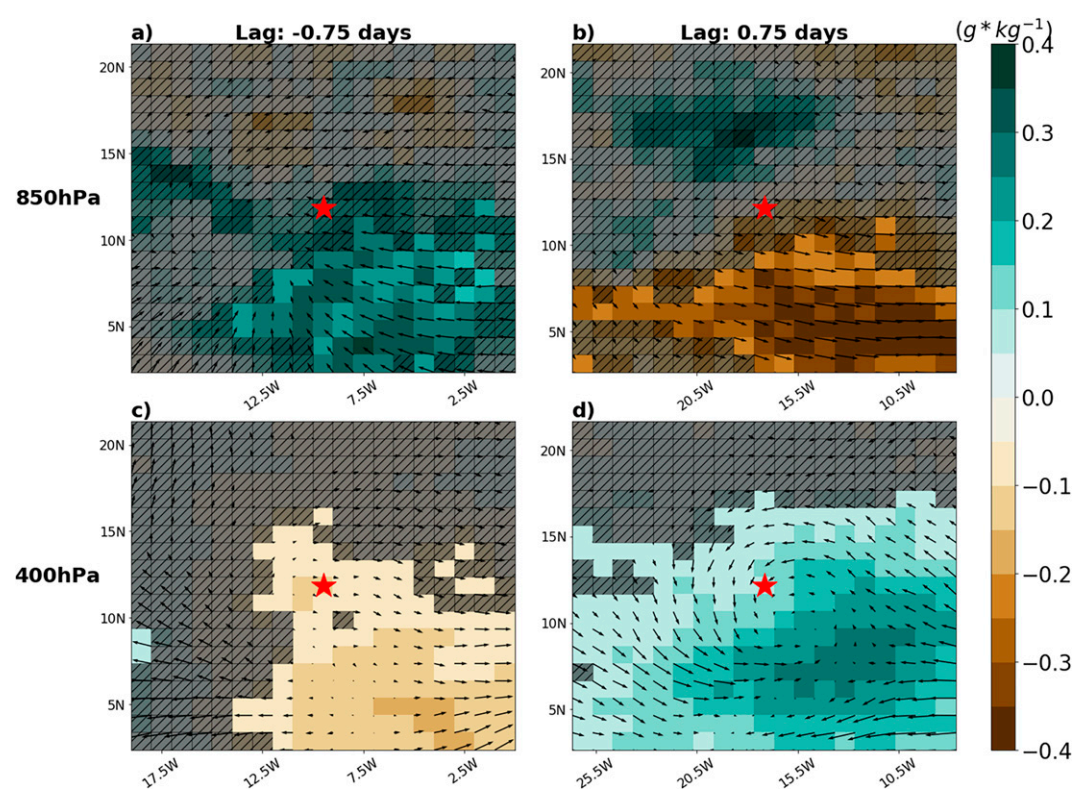


FIG. 10. Differences in lagged spatial composites of specific humidity, comparing different lag times and levels. Columns indicate lag times relative to the CCKW crest, and rows indicate levels. (a),(c) The differences in specific humidity composites 0.75 days (18 h) before the CCKW crest for the 850- and 400-hPa levels, respectively. (b),(d) As in (a) and (c), but for 0.75 days (18 h) after the CCKW crest. Black vectors indicate the difference between the active and suppressed wind vectors at the corresponding lag times and levels. Hatched and grayed out boxes are those that do not pass a significance test (for null hypothesis 2) at a 95% threshold.

(Dunkerton et al. 2009; Wang et al. 2010), the enhanced vorticity has already departed the AEW center by day +0.75 and +1. In contrast, the 400-hPa relative vorticity is enhanced +1 day following the active CCKW crest (Fig. 9c) and includes a pronounced meridional component east and west of the AEW center (difference vectors in Fig. 9 and Fig. 10). This enhanced upper-level circulation may be more efficient at retaining enhanced specific humidity within the wave pouch, resulting in a greater spatial coverage of specific humidity anomalies.

An additional cause of the differences in spatial extent could be the control of convection on middle and upper-level specific humidity. As noted previously, convective coverage within 600 km from the AEW center is significantly enhanced for up to +0.5 days following an active CCKW crest (Fig. 5a). Invigorated deep convection could result in increased specific humidity high in the troposphere (600–200 hPa) near the AEW wave trough, helping explain the more poleward extent of 400-hPa specific humidity anomalies.

4. Relative importance and attribution of CCKW signals

While these results indicate that CCKWs influence AEWs, they do not directly show how impactful this influence is.

Furthermore, it is valuable to determine if CCKWs only provide a transient boost to AEWs or if their impacts are sustained through feedbacks within the AEW system. In this section we address the relative importance of the aforementioned composites and attempt to separate out the AEW- and CCKW-related signals.

a. Relative importance of environmental variables

Ultimately, CCKWs are just one phenomenon that can modify AEWs. To illustrate this point, binned distributions of three AEW characteristics (taken at 400 hPa and a +1-day lag) are shown for the active and suppressed samples in Fig. 11. While the composited means for each of the three highlighted characteristics are indeed different—all passed the significance test for null hypothesis 2 at a 95% threshold (Figs. 5b, 6c, 7c)—there is still a pronounced overlap in the associated distributions. This highlights that CCKWs are not the only thing affecting AEW characteristics.

Another consideration is the relative importance of CCKW-related modifications to AEWs. Table 2 illustrates this by comparing the maximum difference in active-suppressed composites to the typical anomalies surrounding AEWs for multiple variables and levels. Notably, the magnitude of

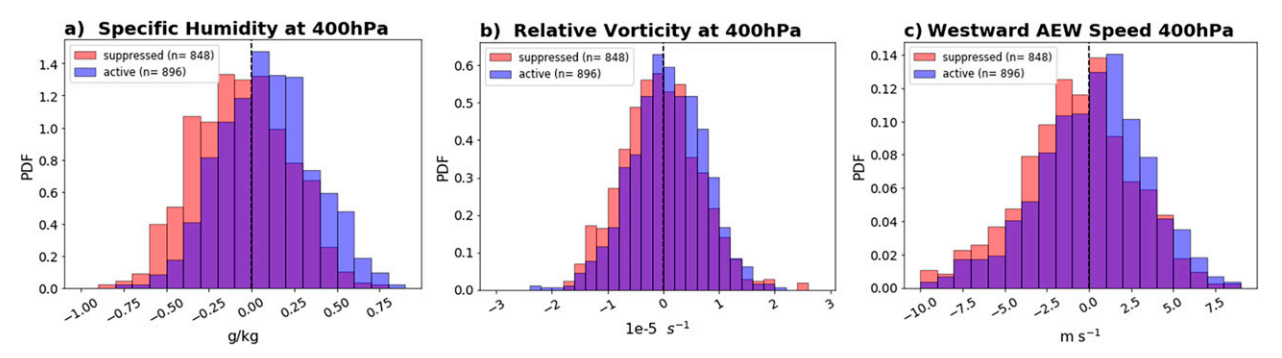


FIG. 11. Histograms showing the PDF of (a) specific humidity, (b) relative vorticity, and (c) westward AEW propagation speed for samples at 400 hPa and day +1 (1 day following the CCKW crest). Data in (a) and (b) are averaged within 600 km of the AEW center. Red bars indicate the suppressed composites, blue bars indicate the active composites, and purple is where these two bars overlap.

CCKW-related deviations is less than one standard deviation of the AEW variability. These data also suggest that the influence of CCKWs on specific humidity and vorticity could be more important at higher levels of the troposphere (400 hPa) compared with lower levels (700 and 850 hPa). Climatologically, AEW-related vorticity and moisture anomalies are typically not as developed at higher levels, and thus CCKWs may have an outsized impact. This is exemplified in specific humidity, where the maximum active-suppressed difference at 400 hPa was over 150% of the typical anomaly found for AEWs, and over 50% of the standard deviation. Meanwhile, modifications to the 200-850-hPa wind shear magnitude are in line with changes to the other fields.³ However, its impact may be understated here due to the study region encompassing different background wind shear regimes.

b. Attribution of AEW response

So far, composites have represented the combined effects of overlapping CCKWs and AEWs. One way to try and separate CCKW-related signals from those directly associated with AEWs is by filtering out eastward-propagating and westward-propagating signals and building the same vertical composites as in section 3a (Fig. 12). Here, composite differences are built in the left column (Figs. 12a,c) using only eastward-propagating signals, and in the second column (Figs. 12b,d) using only westward-propagating signals.

When comparing the center and left columns of Fig. 12, it is clear the vorticity and specific humidity responses are dominated by the eastward-propagating signals (Figs. 12a,c), as the magnitudes of the westward-propagating signals (Figs. 12b,e) are much smaller. This likely indicates that observed environmental changes near the AEW trough (Fig. 6c and Fig. 7c) are dominated by a superposition of CCKW-related signals.

However, when westward-propagating composites are subset to include only the top 50% of AEWs by strength (Figs. 12c,f), the magnitude of the westward-propagating *vorticity* response is larger. This may hint at the long-term impacts CCKWs have on barotropic AEW growth (Mantripragada et al. 2021). As discussed in the methodology, one caveat of the compositing method is that long-term impacts could get washed out at time lags further from day 0. Nevertheless, the eastward-propagating signals still dominate in the short term.

5. Impact of location and wave strength on composites

The results presented so far have been composited over a large geographical region spanning the African continent and the Atlantic Ocean. However, how the influence of CCKWs on AEWs may change based on region and each wave's strength is of both scientific and operational interest. We now compute similar composites as those in section 3 but subdivided based on the location and strength of AEWs and CCKWs. We will refer to the difference between active and suppressed composites as the "response."

a. Specific humidity

The response of specific humidity around AEWs to CCKWs does appear to be influenced by both the latitude of the AEW and the strength of the passing CCKW (as measured by filtered T_b). The latitudinal influence is illustrated by the specific humidity response for AEWs located at higher latitudes (10°–15°N) compared with those located at lower latitudes (5°–10°N) (Figs. 13a,c). While the response of upper-level specific humidity surrounding the AEW still peaks following an active CCKW crest, the magnitude of this peak is reduced for the more northern AEWs located between 10° and 15°N. Similar results are obtained when comparing 15°–20°N to 5°–10°N. Physically, this appears to be connected to the more equatorward position of the CCKW convective signal, which is

 $^{^3}$ One caveat is that taking the climatology of 200–850-hPa wind shear anomalies for AEWs results in a value that is small in magnitude. This artificially inflates the maximum deviation compared to the AEW mean. When compared to the *non-AEW-adjusted wind shear*, the AEW-relative average becomes 12.8 m s $^{-1}$ and the resulting maximum deviation from the mean is reduced to 6.5%. Standard deviation should, however, be less impacted by this.

⁴ It should be noted that while there are widespread significant differences (not shown) in active and suppressed composites for eastward-filtered signals (Figs. 12a,c), the same is not true for the westward-filtered signals (Figs. 12b,c,e,f).

TABLE 2. Summary of the relative importance of the CCKW influence on AEW variables at different levels, compared with climatological averages and standard deviations. The 60°W–30°E averages are calculated via the anomaly of a variable from the background climatology, averaged within 600 km of AEW centers. Standard deviation is computed similarly (not shown). Relative maximum deviation percentages are calculated by dividing the largest difference in a variable's active–suppressed composites by the corresponding 60°W–30°E average or standard deviation.

Variable	Level (hPa)	60°W–30°E AEW avg	Max deviation relative to mean	Max deviation relative to std dev	Lag time of max deviation (days)
Relative vorticity	400	$2.36 \times 10^{-6} \text{ s}^{-1}$	69.6%	18.8%	1
	700	$1.26 \times 10^{-5} \text{ s}^{-1}$	13.8%	26.8%	0.75
	850	$8.39 \times 10^{-6} \text{ s}^{-1}$	22.7%	27.3%	0
Specific humidity	400	$1.09 \times 10^{-4} \text{ kg kg}^{-1}$	157.1%	57.7%	0.5
	700	$3.78 \times 10^{-4} \text{ kg kg}^{-1}$	43.4%	20.0%	-0.5
	850	$5.18 \times 10^{-4} \text{ kg kg}^{-1}$	23.4%	11.6%	-0.5
Wind shear magnitude (200–850 hPa)	_	-0.42 m s^{-1}	219.3%	23.9%	-1.25

maximized between 5° and 10°N (e.g., Fig. 1b). Previously, we hypothesized that upper-level humidity modulations could be a result of the enhanced convection that occurs with CCKWs. This could explain why most of the statistically significant differences here are concentrated high in the troposphere; an AEW located farther south is likely to have more of its convection modified by CCKWs, leading to higher magnitude change in specific humidity. A similar argument can be made when comparing this humidity response for AEW passages through stronger CCKWs versus weaker CCKWs. As illustrated in Figs. 13b,d, stronger CCKWs appear to result in a more robust specific humidity response at upper levels. Because our measure

of CCKW strength (Kelvin-filtered T_b) is directly linked to convective activity, this suggests that more convectively robust CCKWs are associated with larger variations in the upper-level humidity.

One caveat here is that the latitude of AEWs and AEW-CCKW interactions generally increase in the western portions of the domain (Figs. 1a, 4a). However, similar patterns to those in Figs. 13c,d are obtained when restricting passages to be east of 40° or 18°W (not shown). Additionally, we found no statistically significant differences in the specific humidity response comparing longitude subsets (not shown).

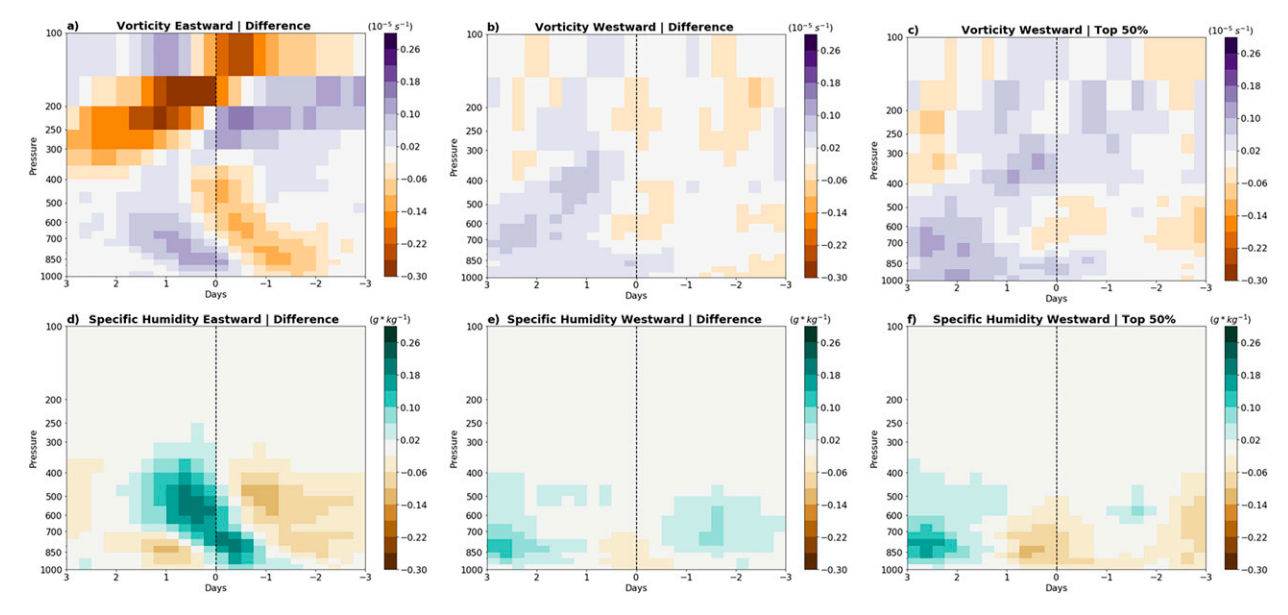


FIG. 12. Vertical cross sections showing differences in lagged filtered composites of relative vorticity and specific humidity averaged within 600 km of the AEW center. (a),(b) As in Fig. 6c, but filtering to retain only the eastward- and westward-propagating components of relative vorticity, respectively. (d),(e) As in (a) and (b), but for specific humidity. (c),(f) As in (b) and (e), but only including the top 50% of samples as measured by AEW strength. Strength is measured by the 700-hPa modified curvature vorticity averaged within 600 km of the AEW center, over its lifetime.

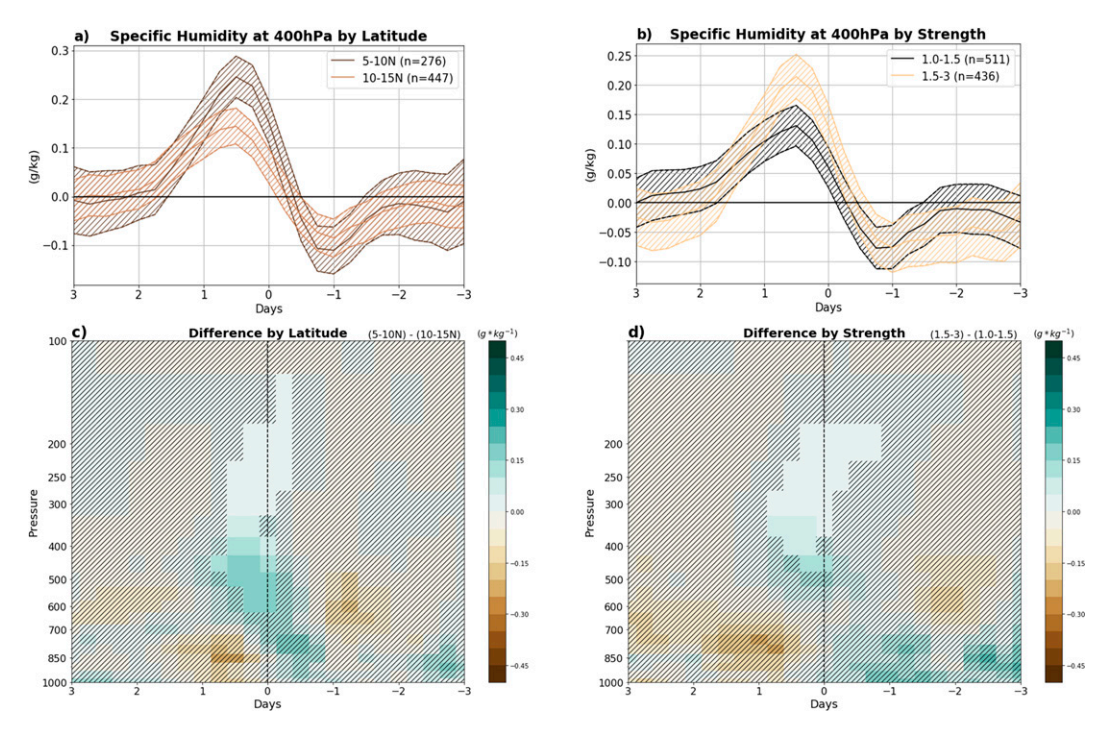


FIG. 13. Comparison of the difference in composites of specific humidity when separated into subsets. Specific humidity here is averaged within 600 km of the AEW center. (a) Comparison of the difference in active–suppressed composites of 400-hPa specific humidity for passages located between latitudes 5° and 10°N (dark brown) and passages between latitudes 10° and 15°N (light brown). Hatched region surrounding each line is the bootstrapped 95% confidence interval (for the modified null hypothesis 2). (b) As in (a), but comparing responses for weak CCKWs [1–1.5 standard deviations (STD), black] and stronger CCKWs (1.5–3 STD, yellow). (c) As in (a), but for all levels and subtracting the 10°–15°N subset from the 5°–10°N subset. (d) As in (b), but for all levels and subtracting the 1–1.5 STD CCKW strength subset from the 1.5–3 STD subset. For (c) and (d), nonsignificant differences between subsets are hatched out.

b. Wind shear

Earlier, it was shown that taken across the entire analysis domain (60°W-30°E), the magnitude of the wind shear response was fairly weak (Fig. 5c, Table 2). This is partially due to the difference in wind shear regimes over the western Atlantic compared with the eastern Atlantic and Africa, as was first suggested by Ventrice et al. (2012b). This relationship becomes more evident when separating AEW-CCKW passages by longitude (Figs. 14a,b). While the magnitude of wind shear surrounding AEWs increases from days 0 to +2 for passages that occur over West Africa (20°-0°W), this effect is largely absent for passages occurring over the eastern Atlantic (40°-20°W) and switches over to a wind shear reduction over the western Atlantic (Figs. 14a,b). As suggested by Ventrice et al. (2012b), this is likely a result of the CCKW-related zonal wind anomalies (positive anomalies in lower troposphere, negative in upper troposphere) adding to climatological easterly shear for passages over the African continent and opposing climatological westerly shear over the western Atlantic. Furthermore, the magnitudes of these wind shear anomalies reach approximately $\pm 1 \text{ m s}^{-1}$ at their peak (around days +1 to +1.5), greater than what is obtained when averaging over the whole domain (Fig. 5c, ~0.75 m s⁻¹). No significant difference in response is seen when comparing passages

between 5°-10°N and 10°-15°N (Fig. 14c). We also do not find significant differences when dividing subsets by CCKW strength (not shown).

c. Vorticity

Surprisingly, the relative vorticity does not exhibit significant differences when CCKW strength and AEW latitude subsets were compared (not shown). However, the relative vorticity response at middle levels (600–700 hPa) appears to be of a higher magnitude and lasts for a longer period of time when subsets of stronger AEWs are included (Fig. 15). When only including the strongest 50% of AEWs for active and suppressed composites (Fig. 15a), the statistically significant regions extend through day +2 with a higher magnitude response than originally seen (cf. Fig. 6c). The response is even larger when including the top 25% of waves (Fig. 15b), though the more limited sample size shrinks the area of significant changes. The

⁵ Interestingly, a significant difference between the 5°–10°N and the 15°–20°N passages is seen, with the latter showing a reduction in wind shear magnitude from days 0 to +2. We hypothesize that this can be attributed to the confounding of latitude with longitude, as most 15°–20°N passages are concentrated in the western Atlantic (see Fig. 4).

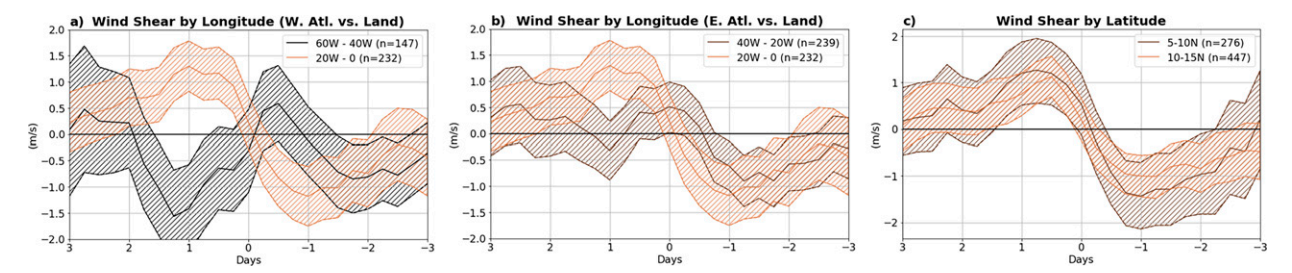


FIG. 14. Comparison of differences in composited 200–850-hPa wind shear magnitude, subset by (a),(b) longitude and (c) latitude. Wind shear is computed within a 600-km radius of the AEW center. (a) Comparison of the difference in active–suppressed composites of wind shear magnitude for passages located between longitudes 60° and 40°W (black) with those located between longitudes 20°W and 0° (light brown). (b) As in (a), but comparing responses for passages located between 40° and 20°W (dark brown) with those located between 20°W and 0° (light brown). (c) As in (b), but comparing passages between 5° and 10°N (dark brown) with those located between 10° and 15°N (light brown). As in Fig. 13, hatching around each composite line indicates the bootstrapped 95% confidence interval (for the modified null hypothesis 2).

interpretation of these results could be slightly confounded by selecting for stronger AEWs. However, there is reason to believe that eliminating weak or dissipating AEWs could better highlight a longer-term AEW response to CCKWs. The presence of a longer-lasting increase in AEW strength is supported by recent findings by Mantripragada et al. (2021).

6. Discussion and conclusions

In this analysis, we used an objective AEW tracker and spatiotemporal filtering of T_b to build a database of AEW–CCKW passages for 1981–2019. We actively excluded AEWs that developed into TCs to prevent the processes specific to TC genesis from biasing composites. Despite this, results for non-developing AEWs are qualitatively similar to past studies of tropical cyclogenesis (Ventrice et al. 2012a; Schreck 2015, 2016). This suggests that CCKWs impact developing AEWs in a similar manner to what is shown here. Further supporting this, we find that the strongest non-developing AEWs (e.g., Fig. 15) display qualitatively similar responses to those of weaker waves, as do composites including all AEWs and those of developing AEWs on their own (not shown). It is cautioned, however, that while we anticipate that the results presented

here are relevant for developing AEWs, further investigation is needed to corroborate this.

Importantly, we confirm that many of the results illustrated by Schreck (2015, 2016) and Ventrice et al. (2012a,b) for pre-TC disturbances are also applicable to non-developing AEWs. Relative vorticity surrounding the AEW trough increases following the active CCKW crest, and the response is tilted westward such that the largest magnitudes at middle and upper levels (700–300 hPa) are seen +0.5 to +1.5 days following the CCKW crest. The reverse happens following suppressed CCKW crests, with relative vorticity decreasing. As Schreck (2016) found for pre-TC disturbances, these relative vorticity modifications can be attributed to CCKW-induced zonal wind anomalies. CCKWs also appear to modify wind shear around AEWs and do so differently depending on the background wind shear regime. This follows what was hypothesized by Ventrice et al. (2012b).

Several results provide deeper insights into the AEW-CCKW relationship and could hint at implications to TC genesis processes. Convective coverage (areal extent of $T_b < 240 \mathrm{K}$) surrounding the AEW trough changed in phase with CCKW crests. This is important because previous work has shown that increased convective coverage is a key precursor to TC

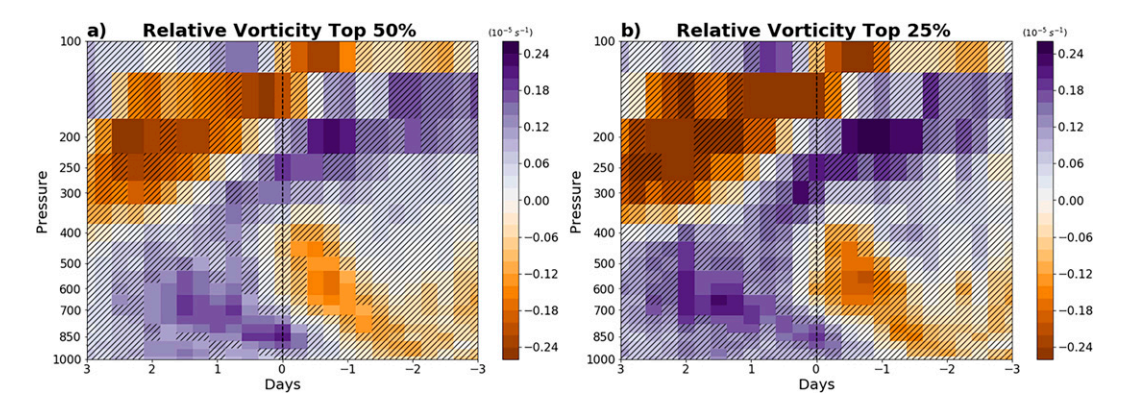


FIG. 15. As in Fig. 6c, but (a) only including the top 50% of AEWs by strength and (b) the top 25% of AEWs by strength. Strength is measured by the 700-hPa modified curvature vorticity averaged within 600 km of the AEW center, and the subsets here are chosen based on average values throughout a AEW's lifetime.

genesis events (Leppert et al. 2013a,b; Zawislak and Zipser 2014). Additionally, a decrease in westward AEW propagation speed is observed following the suppressed phase of CCKWs. We hypothesize that reduced convective coverage could allow for a decoupling of the lower levels of the AEW from upper levels, diminishing the influence of middle and upper-level easterlies on westward propagation (Russell et al. 2020; Russell and Aiyyer 2020). It could also limit AEW propagation directly tied to convective processes (e.g., Russell et al. 2020). Furthermore, specific humidity surrounding AEWs increases following the active CCKW crest, and the response is tilted in a similar manner to that of relative vorticity. We observe a more spatially extensive specific humidity response at mid- to upper levels compared with that at lower levels, possibly related to the distribution of specific humidity by CCKWassociated convection. One reason these observed changes to specific humidity could be important is that increased moisture is known to help TC genesis and intensification processes (Zawislak and Zipser 2014; Tang and Emanuel 2012; Nolan

These results provide more evidence as to why the favorable phasing of CCKWs for TC genesis lags a few days behind the CCKW active phase (Ventrice et al. 2012a, Schreck 2015). CCKWs help increase midlevel moisture and mid- to upper-level relative vorticity in middle and upper levels surrounding AEWs for up to 1.5 days following an active CCKW phase, and even longer for vorticity when excluding the weakest AEWs. Prior to this, an active CCKW phase can temporarily increase the spatial coverage of convection around the AEW and amplify low-level convergence. If these factors also occur for developing AEWs, which we argue is likely, they could increase the favorability of the background environment to TC genesis. Another interesting result is that being at a lower latitude and encountering a stronger CCKW could amplify the specific humidity response around AEWs.

When building composites for eastward- and westward-filtered signals (Fig. 12), we demonstrate that most of the changes found in this analysis were confined to eastward-moving signals (likely associated with CCKWs). However, limiting composites to stronger AEWs caused the magnitude of the westward-moving CCKW response to increase. This suggests that CCKWs could be modifying AEW growth processes, as has been suggested by previous studies (Ventrice and Thorncroft 2013; Mantripragada et al. 2021). However, it still appears that this effect is overshadowed in the short-term by the superposition of CCKW related signals. We hypothesize that these short-term effects are the most important for TC genesis, which is the subject of future work.

We have demonstrated that CCKWs have a pronounced impact on non-developing AEWs. This suggests that CCKWs could modulate AEW impacts and predictability. AEWs contribute strongly to rainfall variability over Africa (Diedhiou et al. 1999; Mekonnen et al. 2006), implying that interactions with CCKWs may contribute to their societal impacts in this region. Furthermore, convective and intensity differences in AEWs have been shown to affect ensemble model predictions of AEWs (Elless and Torn 2018, 2019). At the moment, a connection between CCKWs and increased AEW forecasting

error has not been established, and recent work suggests it could be minimal (Elless and Torn 2019). Nevertheless, with the now well-established role of convection in AEW growth and propagation (Russell et al. 2020; Russell and Aiyyer 2020), further investigation of this is warranted. More research is also needed to better establish the connections between CCKWs and the processes governing AEW dynamics. These questions could be addressed with the use of numerical models and a more detailed satellite analysis in the future.

Acknowledgments. We thank James Russell, Rosimar Rios-Berrios, Alan Brammer, Travis Elless, and Ryan Torn for helpful discussions that improved this paper. Feedback from Anantha Aiyyer and two anonymous reviewers also helped greatly improve this work. This project was supported by NSF Grant AGS-1747781 and through an NSF Graduate Research Fellowship (1938060). Schreck acknowledges NASA Grant NNX17AH61G.

Data availability statement. ERA5 data utilized in this study are available online and were obtained via the Copernicus Climate Data Store at http://cds.climate.copernicus.eu (see Hersbach et al. 2020). GridSat-B1 satellite data were obtained via https://www.ncdc.noaa.gov/gridsat/gridsat-index.php (see Knapp et al. 2011). Objective AEW tracks and corresponding CCKW crest locations used in this study, along with the corresponding python code, are publicly available in a repository at http://doi.org/10.17605/OSF.IO/J4HPQ. An advanced technical description of the code is provided there. This repository also contains the AEW-following data used to build composites presented in this paper.

REFERENCES

- Avila, L. A., R. J. Pasch, and J.-G. Jiing, 2000: Atlantic tropical systems of 1996 and 1997: Years of contrasts. *Mon. Wea. Rev.*, **128**, 3695–3706, https://doi.org/10.1175/1520-0493(2000) 128<3695:ATSOAY>2.0.CO:2.
- Bain, C. L., K. D. Williams, S. F. Milton, and J. T. Heming, 2014: Objective tracking of African easterly waves in Met Office models. *Quart. J. Roy. Meteor. Soc.*, 140, 47–57, https://doi. org/10.1002/qj.2110.
- Berry, G. J., and C. D. Thorncroft, 2012: African easterly wave dynamics in a mesoscale numerical model: The upscale role of convection. J. Atmos. Sci., 69, 1267–1283, https://doi.org/10. 1175/JAS-D-11-099.1.
- —, C. Thorncroft, and T. Hewson, 2007: African easterly waves during 2004—Analysis using objective techniques. *Mon. Wea. Rev.*, 135, 1251–1267, https://doi.org/10.1175/MWR3343.1.
- Bessafi, M., and M. C. Wheeler, 2006: Modulation of South Indian Ocean tropical cyclones by the Madden–Julian oscillation and convectively coupled equatorial waves. *Mon. Wea. Rev.*, **134**, 638–656, https://doi.org/10.1175/MWR3087.1.
- Brammer, A., and C. D. Thorncroft, 2015: Variability and evolution of African easterly wave structures and their relationship with tropical cyclogenesis over the eastern Atlantic. *Mon. Wea. Rev.*, 143, 4975–4995, https://doi.org/10.1175/MWR-D-15-0106.1.

- —, and J. P. Dunion, 2018: Observations and predictability of a nondeveloping tropical disturbance over the eastern Atlantic. *Mon. Wea. Rev.*, **146**, 3079–3096, https://doi.org/10.1175/MWR-D-18-0065.1.
- Burpee, R. W., 1972: The origin and structure of easterly waves in the lower troposphere of North Africa. *J. Atmos. Sci.*, **29**, 77–90, https://doi.org/10.1175/1520-0469(1972)029<0077: TOASOE>2.0.CO;2.
- Chen, T.-C., S.-Y. Wang, and A. J. Clark, 2008: North Atlantic hurricanes contributed by African easterly waves north and south of the African easterly jet. *J. Climate*, 21, 6767–6776, https://doi.org/10.1175/2008JCLI2523.1.
- Cheng, Y.-M., C. D. Thorncroft, and G. N. Kiladis, 2019: Two contrasting African easterly wave behaviors. *J. Atmos. Sci.*, **76**, 1753–1768, https://doi.org/10.1175/JAS-D-18-0300.1.
- Diedhiou, A., S. Janicot, A. Vitard, P. de Felice, and H. Laurent, 1999: Easterly wave regimes and associated convection over West Africa and tropical Atlantic: Results from the NCEP/ NCAR and ECMWF reanalyzes. *Climate Dyn.*, 15, 795–822, https://doi.org/10.1007/s003820050316.
- Dunkerton, T. J., M. T. Montgomery, and Z. Wang, 2009: Tropical cyclogenesis in a tropical wave critical layer: Easterly waves. *Atmos. Chem. Phys.*, 9, 5587–5646, https://doi.org/10.5194/acp-9-5587-2009.
- Elless, T. J., and R. D. Torn, 2018: African easterly wave forecast verification and its relation to convective errors within the ECMWF ensemble prediction system. *Wea. Forecasting*, **33**, 461–477, https://doi.org/10.1175/WAF-D-17-0130.1.
- —, and —, 2019: Investigating the factors that contribute to African easterly wave intensity forecast uncertainty in the ECMWF ensemble prediction system. *Mon. Wea. Rev.*, **147**, 1679–1698, https://doi.org/10.1175/MWR-D-18-0071.1.
- Emanuel, K. A., D. J. Neelin, and C. Bretherton, 1994: On large-scale circulations in convecting atmosphere. *Quart. J. Roy. Meteor. Soc.*, **120**, 1111–1143, https://doi.org/10.1002/qj.49712051902.
- Frank, W. M., and P. E. Roundy, 2006: The role of tropical waves in tropical cyclogenesis. *Mon. Wea. Rev.*, **134**, 2397–2417, https://doi.org/10.1175/MWR3204.1.
- Gruber, A., 1974: The wavenumber-frequency spectra of satellite-measured brightness in the tropics. *J. Atmos. Sci.*, **31**, 1675–1680, https://doi.org/10.1175/1520-0469(1974)031<1675: TWFSOS>2.0.CO;2.
- Hall, N. M., G. N. Kiladis, and C. D. Thorncroft, 2006: Three-dimensional structure and dynamics of African easterly waves. Part II: Dynamical modes. J. Atmos. Sci., 63, 2231–2245, https://doi.org/10.1175/JAS3742.1.
- Hankes, I., Z. Wang, G. Zhang, and C. Fritz, 2015: Merger of African easterly waves and formation of Cape Verde storms. *Quart. J. Roy. Meteor. Soc.*, 141, 1306–1319, https://doi.org/10. 1002/qj.2439.
- Hersbach, H., and Coauthors, 2020: The ERA5 global reanalysis. *Quart. J. Roy. Meteor. Soc.*, **146**, 1999–2049, https://doi.org/10.1002/qj.3803.
- Hopsch, S. B., C. D. Thorncroft, and K. R. Tyle, 2010: Analysis of African easterly wave structures and their role in influencing tropical cyclogenesis. *Mon. Wea. Rev.*, 138, 1399–1419, https:// doi.org/10.1175/2009MWR2760.1.
- Janiga, M. A., and C. D. Thorncroft, 2013: Regional differences in the kinematic and thermodynamic structure of African easterly waves. *Quart. J. Roy. Meteor. Soc.*, 139, 1598–1614, https://doi.org/10.1002/qj.2047.

- —, and —, 2016: The influence of African easterly waves on convection over tropical Africa and the east Atlantic. *Mon. Wea. Rev.*, **144**, 171–192, https://doi.org/10.1175/MWR-D-14-00419.1.
- Kiladis, G. N., C. D. Thorncroft, and N. M. Hall, 2006: Three-dimensional structure and dynamics of African easterly waves. Part I: Observations. J. Atmos. Sci., 63, 2212–2230, https://doi.org/10.1175/JAS3741.1.
- —, M. C. Wheeler, P. T. Haertel, K. H. Straub, and P. E. Roundy, 2009: Convectively coupled equatorial waves. *Rev. Geophys.*, 47, RG2003, https://doi.org/10.1029/2008RG000266.
- Knapp, K. R., and Coauthors, 2011: Globally gridded satellite (GridSat) observations for climate studies. *Bull. Amer. Meteor.* Soc., 92, 893–907, https://doi.org/10.1175/2011BAMS3039.1.
- Landsea, C. W., and J. L. Franklin, 2013: Atlantic hurricane database uncertainty and presentation of a new database format. *Mon. Wea. Rev.*, 141, 3576–3592, https://doi.org/10. 1175/MWR-D-12-00254.1.
- Leppert, K. D., II, D. J. Cecil, and W. A. Petersen, 2013a: Relation between tropical easterly waves, convection, and tropical cyclogenesis: A Lagrangian perspective. *Mon. Wea. Rev.*, 141, 2649–2668, https://doi.org/10.1175/MWR-D-12-00217.1.
- ——, W. A. Petersen, and D. J. Cecil, 2013b: Electrically active convection in tropical easterly waves and implications for tropical cyclogenesis in the Atlantic and East Pacific. *Mon. Wea. Rev.*, 141, 542–556, https://doi.org/10.1175/MWR-D-12-00174.1.
- Liebmann, B., G. N. Kiladis, L. M. V. Carvalho, C. Jones, C. S. Vera, I. Bladé, and D. Allured, 2009: Origin of convectively coupled Kelvin waves over South America. *J. Climate*, 22, 300–315, https://doi.org/10.1175/2008JCL12340.1.
- Mantripragada, R. S. S., C. J. Schreck III, and A. Aiyyer, 2021: Energetics of interactions between African easterly waves and convective coupled Kelvin waves. *Mon. Wea. Rev.*, 149, 3821–3835, https://doi.org/10.1175/MWR-D-21-0003.1.
- Mayta, V. C., G. N. Kiladis, J. Dias, P. L. S. Dias, and M. Gehne, 2021: Convectively coupled Kelvin waves over tropical South America. J. Climate, 34, 6531–6547, https://doi.org/10.1175/ JCLI-D-20-0662.1.
- Mekonnen, A., C. D. Thorncroft, and A. R. Aiyyer, 2006: Analysis of convection and its association with African easterly waves. *J. Climate*, 19, 5405–5421, https://doi.org/10.1175/JCLI3920.1.
- —, —, and G. N. Kiladis, 2008: Convectively coupled Kelvin waves over tropical Africa during the boreal summer: Structure and variability. *J. Climate*, 21, 6649–6667, https://doi.org/10.1175/2008JCLI2008.1.
- Mounier, F., G. Kiladis, and S. Janicot, 2007: Analysis of the dominant mode of convectively coupled Kelvin waves in the West African monsoon. *J. Climate*, 20, 1487–1503, https://doi.org/10.1175/JCLI4059.1.
- Nolan, D. S., 2007: What is the trigger for tropical cyclogenesis? Aust. Meteor. Mag., 56, 241–266.
- Núñez Ocasio, K. M., J. L. Evans, and G. S. Young, 2020: A wave-relative framework analysis of AEW–MCS interactions leading to tropical cyclogenesis. *Mon. Wea. Rev.*, 148, 4657–4671, https://doi.org/10.1175/MWR-D-20-0152.1.
- —, A. Brammer, J. L. Evans, G. S. Young, and Z. L. Moon, 2021: Favorable monsoon environment over eastern Africa for subsequent tropical cyclogenesis of African easterly waves. J. Atmos. Sci., 78, 2911–2925, https://doi.org/10.1175/ JAS-D-20-0339.1.

- Peng, M. S., B. Fu, T. Li, and D. E. Stevens, 2012: Developing versus nondeveloping disturbances for tropical cyclone formation. Part I: North Atlantic. *Mon. Wea. Rev.*, 140, 1047–1066, https://doi.org/10.1175/2011MWR3617.1.
- Reed, R. J., D. C. Norquist, and E. E. Recker, 1977: The structure and properties of African wave disturbances as observed during phase III of GATE. *Mon. Wea. Rev.*, **105**, 317–333, https://doi.org/10.1175/1520-0493(1977)105<0317: TSAPOA>2.0.CO;2.
- Russell, J. O., and A. Aiyyer, 2020: The potential vorticity structure and dynamics of African easterly waves. *J. Atmos. Sci.*, **77**, 871–890, https://doi.org/10.1175/JAS-D-19-0019.1.
- —, —, J. D. White, and W. Hannah, 2017: Revisiting the connection between African easterly waves and Atlantic tropical cyclogenesis. *Geophys. Res. Lett.*, 44, 587–595, https://doi.org/10.1002/2016GL071236.
- —, and —, 2020: African easterly wave dynamics in convection-permitting simulations: Rotational stratiform instability as a conceptual model. *J. Adv. Model. Earth Syst.*, **12**, e2019MS001706, https://doi.org/10.1029/2019MS001706.
- Schreck, C. J., 2015: Kelvin waves and tropical cyclogenesis: A global survey. Mon. Wea. Rev., 143, 3996–4011, https://doi. org/10.1175/MWR-D-15-0111.1.
- —, 2016: Convectively coupled Kelvin waves and tropical cyclogenesis in a semi-Lagrangian framework. *Mon. Wea. Rev.*, 144, 4131–4139, https://doi.org/10.1175/MWR-D-16-0237.1.
- Straub, K. H., and G. N. Kiladis, 2002: Observations of a convectively coupled Kelvin wave in the eastern Pacific ITCZ. J. Atmos. Sci., 59, 30–53, https://doi.org/10.1175/1520-0469(2002) 059<0030:OOACCK>2.0.CO;2.
- —, and —, 2003: Extratropical forcing of convectively coupled Kelvin waves during austral winter. *J. Atmos. Sci.*, **60**, 526–543, https://doi.org/10.1175/1520-0469(2003)060
 0526:EFOCCK>2.0.CO;2.
- Takayabu, Y. N., 1994: Large-scale cloud disturbances associated with equatorial waves. Part I: Spectral features of the cloud disturbances. J. *Meteor. Soc. Japan*, **72**, 433–449, https://doi.org/10.2151/jmsj1965.72.3_433.
- Tang, B., and K. Emanuel, 2012: A ventilation index for tropical cyclones. *Bull. Amer. Meteor. Soc.*, 93, 1901–1912, https://doi. org/10.1175/BAMS-D-11-00165.1.
- Thorncroft, C. D., N. M. J. Hall, and G. N. Kiladis, 2008: Threedimensional structure and dynamics of African easterly waves.

- Part III: Genesis. J. Atmos. Sci., 65, 3596–3607, https://doi.org/ 10.1175/2008JAS2575.1.
- Ventrice, M. J., and C. D. Thorncroft, 2013: The role of convectively coupled atmospheric Kelvin waves on African easterly wave activity. *Mon. Wea. Rev.*, 141, 1910–1924, https://doi.org/10.1175/MWR-D-12-00147.1.
- —, and M. A. Janiga, 2012a: Atlantic tropical cyclogenesis: A three-way interaction between an African easterly wave, diurnally varying convection, and a convectively coupled atmospheric Kelvin wave. *Mon. Wea. Rev.*, 140, 1108–1124, https://doi.org/10.1175/MWR-D-11-00122.1.
- —, —, and C. Schreck, 2012b: Impacts of convectively coupled Kelvin waves on environmental conditions for Atlantic tropical cyclogenesis. *Mon. Wea. Rev.*, **140**, 2198–2214, https://doi.org/10.1175/MWR-D-11-00305.1.
- Wang, Z., M. T. Montgomery, and T. J. Dunkerton, 2010: Genesis of pre-Hurricane Felix (2007). Part I: The role of the easterly wave critical layer. J. Atmos. Sci., 67, 1711–1729, https://doi. org/10.1175/2009JAS3420.1.
- Wheeler, M., and G. Kiladis, 1999: Convectively coupled equatorial waves: Analysis of clouds and temperature in the wavenumber–frequency domain. J. Atmos. Sci., 56, 374–399, https://doi.org/10.1175/1520-0469(1999)056<0374:CCEWAO>2. 0.CO:2.
- Wu, L., and M. Takahashi, 2017: Contributions of tropical waves to tropical cyclone genesis over the western North Pacific. *Climate Dyn.*, **50**, 4635–4649, https://doi.org/10.1007/s00382-017-3895-3.
- Yanai, M., S. Esbensen, and J.-H. Chu, 1973: Determination of bulk properties of tropical cloud clusters from largescale heat and moisture budgets. J. Atmos. Sci., 30, 611–627, https://doi.org/10.1175/1520-0469(1973)030<0611: DOBPOT>2.0.CO;2.
- Zawislak, J., 2020: Global survey of precipitation properties observed during tropical cyclogenesis and their differences compared to nondeveloping disturbances. *Mon. Wea. Rev.*, 148, 1585–1606, https://doi.org/10.1175/MWR-D-18-0407.1.
- —, and E. J. Zipser, 2014: A multisatellite investigation of the convective properties of developing and nondeveloping tropical disturbances. *Mon. Wea. Rev.*, **142**, 4624–4645, https://doi. org/10.1175/MWR-D-14-00028.1.